Polarimetric Radar Observations of Convection in Northwestern Mexico during the North American Monsoon Experiment

TIMOTHY J. LANG AND STEVEN A. RUTLEDGE

Department of Atmospheric Science, Colorado State University, Fort Collins, Colorado

ROBERT CIFELLI

Cooperative Institute for Research in the Atmosphere, Colorado State University, and NOAA/Earth System Research Laboratory, Boulder, Colorado

(Manuscript received 3 December 2009, in final form 29 April 2010)

ABSTRACT

The spatial and temporal variability of convection during the North American Monsoon Experiment (NAME) was examined via analysis of three-dimensional polarimetric radar data. Terrain bands were defined as the Gulf of California (over water) and elevations of 0–500 m above mean sea level (MSL; coastal plain), 500–1500 m MSL, and >1500 m MSL. Convective rainfall over the Gulf typically featured the smallest values of median volume diameter (D_0) regardless of rain rate. Gulf convection also contained reduced precipitation-sized ice water mass but proportionally more liquid water mass compared to convection over land. These maritime characteristics were magnified during disturbed meteorological regimes, which typically featured increased precipitation over the Gulf and adjacent coastal plain. Overall, the results suggest increased reliance on warm-rain collision and coalescence at the expense of ice-based precipitation growth processes for convective rainfall over the Gulf, relative to the land. Over land D_0, ice, and liquid water mass all increased with decreasing terrain elevation, suggesting intensification of convection as it moved off the Sierra Madre Occidental. The results are consistent with the hypothesis that both warm-rain and ice-based rainfall processes play important roles in precipitation formation over land. Coastal-plain convection underwent microphysical modifications during disturbed meteorological regimes that were similar to Gulf convection, but the changes were less dramatic. High-terrain convection experienced little microphysical variability regardless of meteorological regime.

1. Introduction

a. Background

There are two generally accepted archetypes for tropical convection: continental and maritime (Rutledge et al. 1992; Williams et al. 1992; Randell et al. 1994; Zipser 1994; Zipser and Lutz 1994; Rosenfeld and Lensky 1998; Nesbitt et al. 2000, 2006; Petersen and Rutledge 2001; Rosenfeld and Ulbrich 2003; Takahashi and Shimura 2004; Phillips et al. 2007; Ulbrich and Atlas 2007; Xu et al. 2009). The continental archetype is characterized by relatively less dependence on ''warm-rain'' microphysical processes, namely collision and coalescence, for the production of rainfall. Instead, continental convection tends to strongly involve ice-based growth processes—in particular, depositional, aggregrational, and riming growth of ice particles, which subsequently melt into rain (Rosenfeld and Lensky 1998; Atlas and Williams 2003; Ulbrich and Atlas 2007). By contrast, the maritime archetype depends more strongly on warm-rain processes (Jorgensen and LeMone 1989; Hu and Srivastava 1995; Rosenfeld and Lensky 1998; Atlas and Ulbrich 2000, 2006; Ulbrich and Atlas 2007). These two archetypes have been invoked to explain, among other things, observed regional variability in latent heating profiles (Tao et al. 2001, 2006, 2010) as well as the observed land–ocean contrast in lightning flash rates (Orville and Spencer 1979; Zipser and Lutz 1994; Boccippio et al. 2000; Nesbitt et al. 2000; Toracinta et al. 2002; Xu et al. 2009).

It is important to note that these convective archetypes merely represent two opposite ends of a spectrum

Corresponding author address: Timothy J. Lang, Dept of Atmospheric Science, Colorado State University, Fort Collins, CO 80523. E-mail: tlang@atmos.colostate.edu

DOI: 10.1175/2010JHM1247.1

of convective microphysical structures (Boccippio et al. 2005). In a given tropical region, one would expect a particular convective storm to exist somewhere along this continuum, with its position on the spectrum defined by the relative importance of warm-rain versus ice-based microphysical processes within it.

Moreover, convection in a particular tropical region need not be composed of only one particular type (Boccippio et al. 2005). Variability in microphysical structure is commonly observed as a function of meteorological forcing. For example, in the Amazon basin easterly low-level winds typically result in convection that is more continental in character, whereas westerly flow results in a more maritime structure (Cifelli et al. 2002, 2004; Halverson et al. 2002; Petersen et al. 2002; Rickenbach et al. 2002; Silva Dias et al. 2002). Another example is in northern Australia, with ''monsoon'' versus ''break'' convection taking on characteristics of the maritime versus continental archetypes, respectively (Rutledge et al. 1992; Williams et al. 1992; Randell et al. 1994; May and Ballinger 2007; May et al. 2008). These are but a few of the many examples of variability in convective structure seen throughout the tropics (Houze and Cheng 1977; Zipser 1994; DeMott and Rutledge 1998; Johnson et al. 1999; Nesbitt et al. 2000; Petersen and Rutledge 2001; Stith et al. 2002; Petersen et al. 2003; Boccippio et al. 2005; Yuter et al. 2005; Cetrone and Houze 2006; Nesbitt et al. 2006; Pereira and Rutledge 2006; Cifelli et al. 2007).

These differences in vertical structure of convection have important impacts on the rainfall drop size distributions (DSDs) observed in convective rainfall. For example, the maritime archetype is characterized by smaller average drop size than in the continental archetype (Atlas and Ulbrich 2000; Bringi et al. 2003, 2009; Rosenfeld and Ulbrich 2003; Atlas and Ulbrich 2006; Ulbrich and Atlas 2007). Understanding and properly characterizing these differences in convective structure and rainfall DSDs is a key goal in precipitation research, especially within the fields of remote sensing and cloud modeling.

Knowledge of convective structure and rainfall is especially important in coastal regions, where both continental and maritime influences exist together. One of the most intriguing tropical coastal regions in the world is the Gulf of California region in northwestern Mexico (Fig. 1). Here, the waters of the Gulf give way to a narrow coastal plain and then up to the 3000-m above mean sea level (MSL) peaks of the Sierra Madre Occidental (SMO) mountain range, all in the span of less than 200 km. This region was the focus of the North American Monsoon Experiment (NAME) during July–August 2004 (Higgins et al. 2006; Higgins and Gochis 2007).

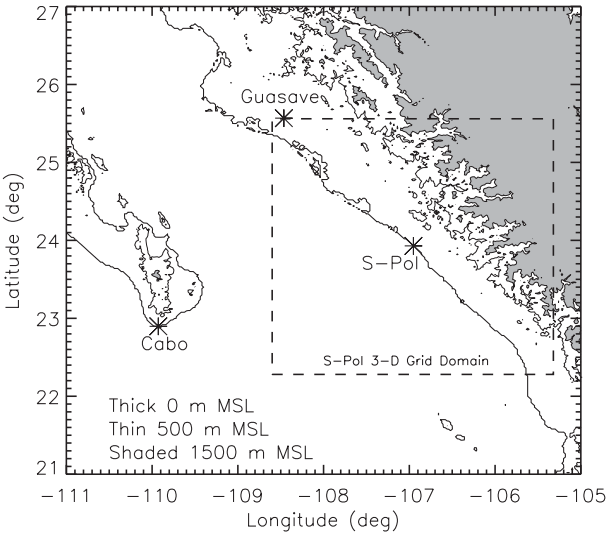

FIG. 1. Map of the NAME region, showing locations of the radar network, the S-Pol 3D grid domain, and topographic bands examined in this study.

NAME involved a large network of sounding stations, profilers, radars, and rain gauges to help characterize convection and convective precipitation in this region. According to Gochis et al. (2007), northwestern Mexican precipitation during the 2004 monsoon season was similar to the long-term climatological average, making this season an excellent choice for studying convection in this region. Results from radar and satellite observations during the project have helped establish that, during the monsoon season, shallow convection begins over the highest peaks of the SMO in the late morning and early afternoon (Lang et al. 2007a; Nesbitt et al. 2008; Rowe et al. 2008). This convection moves westward, intensifying, organizing, and growing upscale as the afternoon progresses. Meanwhile, convection along the sea-breeze front over the coastal plain can start just as early. However, convection normally ends after sunset, with stratiform precipitation and fog common until morning.

The NAME region is regularly affected by transient weather phenomena such as tropical cyclones, gulf surges, easterly waves, and upper-level troughs (Hales 1972; Adams and Comrie 1997; Fuller and Stensrud 2000; Bordoni and Stevens 2006; Higgins et al. 2006). During these disturbed meteorological regimes, convection does not end after sunset; rather, it continues intensifying and organizing well into the nighttime hours as it moves across the coastal plain to the Gulf (Lang et al. 2007a). Moreover, early morning precipitation becomes more common over the Gulf, possibly organizing along a land breeze or evolving from precipitation systems moving along the coast from points south. The basic

paradigm is frequent but less intense rainfall over the high terrain, with episodic but more intense rainfall over the Gulf and coastal plain (Gochis et al. 2003, 2004, 2007; Rowe et al. 2008).

As noted by Nesbitt et al. (2008), monsoon rainfall in the NAME region provides between 40% and 80% of the annual water resource (Douglas et al. 1993; Adams and Comrie 1997; Brito-Castillo et al. 2003; Gochis et al. 2006). Thus, there exists a need for improved hydrological prediction and water resource management there. Understanding the relationships among convective structure, DSDs, and rainfall in this region will assist in those efforts, as better microphysical understanding can help improve satellite precipitation estimates as well as parameterizations in numerical models.

b. Hypotheses

An unanswered issue is the relative importance of warm-rain versus ice-based microphysical processes in NAME convection. Does this vary by terrain, particularly land versus sea? Further, do disturbed meteorological regimes significantly affect convective microphysics, relative to convection during undisturbed periods? Do these regime differences vary by terrain as well?

Based on NAME thermodynamic analyses, Johnson et al. (2007, 2010) demonstrated gradual deepening of convection over the land throughout the day, while the majority of convective heating and moistening was confined to lower levels (below 700 hPa or ~3 km above mean sea level) over the Gulf. This implies that ice-based precipitation processes are less important over the Gulf than over land, as these would tend to produce heating and moistening aloft. Meanwhile, the deepening of convection from high terrain to low terrain over land is consistent with the results of Nesbitt et al. (2008) and Rowe et al. (2008). But what effect does this have on the relative importance of ice-based versus warm-rain processes over land, as a function of terrain?

Nesbitt et al. (2008) suggested that the shallow convection over the highest terrain might imply a greater importance for warm-rain processes there, with increasing effects from ice-based precipitation growth as convection deepened toward the coast. However, Rowe et al. (2008) demonstrated that increased warm-cloud depth toward the coast could aid collision and coalescence growth of rainfall and thus explain the observed gradient in precipitation intensity. Indeed, Williams et al. (2007) found evidence for DSD broadening below the freezing-level altitude at a coastal profiler site during NAME, suggesting an important role for warm-rain precipitation growth at low elevations. However, this same profiler also identified regions of graupel up to 10 km MSL in some coastal convection (Lerach et al. 2010).

Therefore, it is reasonable to hypothesize increased roles for both warm-rain and ice-based precipitation development as NAME convection moves off the high terrain. However, there may be a fundamental change in microphysical structure once convection reaches the Gulf, with a transition toward dominance of warm-rain processes over the water. In addition, fundamental changes in convective structure may occur during disturbed meteorological regimes, particularly over the coastal plain and Gulf. This study's aim was to test these hypotheses using a three-dimensional (3D) polarimetric radar dataset from NAME, which can be used to estimate rainfall, differentiate between ice and liquid water, and characterize DSDs.

2. Data and methodology

a. Data quality control and grid generation

The primary data source for this work was obtained by the National Center for Atmospheric Research (NCAR) S-band dual-polarization Doppler radar (S-Pol). The S-Pol was stationed for six weeks near Mazatlan, Mexico during July–August 2004 as part of the NAME field campaign (Higgins et al. 2006; Lang et al. 2007a). The radar operated nearly continuously during this period, in two modes: a more common full-volume mode that provided 360° of coverage over a 15-min period, and a less common ''storm evolution'' mode that observed two or more sector volumes during a 15-min update cycle. During the S-Pol deployment, precipitation was observed essentially daily by the radar, with modulation of intensity and spatial extent by intraseasonal variability (Lang et al. 2007a).

The meticulous quality control (QC) of the raw polarimetric data has been addressed in other publications (Lang et al. 2006, 2007a,b, 2009) and will not be discussed in detail here. The QC process involved—among other things—proper system calibration of reflectivity (Z_H; to within ±1 dB) and differential reflectivity (Z_{DR}; ±0.1 dB), removal of clutter and other nonmeteorological echo, removal of second-trip echo, filtering of differential phase and calculation of specific differential phase (K_{DP}), correction of Z and Z_{DR} for attenuation, and correction of Z and Z_{DR} for partial beam blockage.

Three-dimensional Cartesian grids were created for each available 15-min radar volume throughout the 6-week duration of the S-Pol deployment. During the ~100 h of the project that storm-evolution scanning occurred, only the first sector volume was used to create the grid for that 15-min period. Note that these time periods did not provide 360° of coverage like the more common full-volume scanning but they represented only a small fraction of the S-Pol dataset.

The array size for each grid was $165 \times 165 \times 20$ points. The horizontal grid spacing was 0.02° latitude–longitude (~2 km). The grid spanned −108.6° to −105.32° in longitude and 22.28° to 25.56° in latitude, and was matched with a section of the NAME two-dimensional (2D) regional multiradar composite grids (Lang et al. 2006, 2007a; Rowe et al. 2008), which included near-surface observations from S-Pol and two Mexican weather service radars for easy intercomparison. The vertical grid spacing was 1 km. The first altitude level was 1 km MSL, so the grids covered 1–20 km MSL. The grids were created using NCAR's Sorted Position Radar Interpolator (SPRINT; Mohr and Vaughn 1979; Miller et al. 1986).

Convective–stratiform partitioning was performed by comparing the convective–stratiform partitioned 2D regional multiradar composite grids of Rowe et al. (2008) with the 3D S-Pol grids in the present study. The Rowe et al. (2008) methodology was based on custom tuning of the well-known Yuter and Houze (1998) algorithm to better match NAME precipitating system structure; see Rowe et al. for more details. Because the 2D and 3D grids matched horizontally, and because the 2D regional grid data in the vicinity of S-Pol were mostly from S-Pol (Lang et al. 2007a), this provided accurate partitioning and isolation of convection. All the data in the vertical column associated with a 2D convective pixel were treated as convection. For more information about the 3D S-Pol grids, see Lang et al. (2007b) and Rowe et al. (2008).

To keep the focus of this study from becoming too broad, stratiform precipitation was not analyzed. It may be examined in the future, as it was an important contributor to total rainfall in this region (Lang et al. 2007a). Overall, the number of convectively raining grid columns identified during the entire field project was on the order of several hundred thousand.

b. Analysis methodology

Near-surface rainfall rate was estimated for each grid point following the Colorado State University blended polarimetric algorithm (Cifelli et al. 2002) as applied to later versions of the NAME radar datasets (Lang et al. 2006; Nesbitt et al. 2008; Rowe et al. 2008) and will not be discussed any further given the comprehensive discussions provided by these past publications. Near-surface median volume diameter (D_0) was estimated for each grid point by the equation $D_0 = 1.529 Z_{\mathrm{DR}}^{0.467}$ (Bringi and Chandrasekar 2001, p. 386). Power-law relations between D_0 and Z_{DR} likely have an inherent point-to-point uncertainty around ±0.15 mm (Williams and May 2008). However, the exact D_0 retrieval error structure is not known for NAME because of a lack of quality validation data such as from a disdrometer. If the error structure was unbiased and normally distributed, then the expected value in the mean is 0 and retrieval errors can be disregarded for the purposes of this study since the focus is on mean values of data subsetted via different spatial and temporal criteria (discussed below). However, even if the retrieval error structure was different than normal, any biases that existed in the D_0 (or any other microphysical) retrievals would not be expected to vary spatially or temporally (i.e., the problem is in the algorithm itself, not the meteorology or the quality-controlled polarimetric variables), making relative comparisons between data subsets still valid since every subset would be biased the same way.

In this study, the 95% confidence intervals for mean D_0 were compared among different data subsets. These intervals were estimated assuming the data were distributed normally (i.e., plus or minus roughly twice the standard error). Computing confidence intervals for means assuming a normal distribution usually works well even for nonnormal distributions (Wang 2001), particularly when dealing with hundreds of thousands of samples, as in this study. Indeed, if anything the normal method tends to produce larger confidence interval widths than other methods (Wang 2001), which would make the present study err on the side of extra caution in interpreting results.

Ice water mass and liquid water mass were estimated for all convective grid points following the polarimetric methodology of Carey and Rutledge (2000) and Cifelli et al. (2002). To briefly summarize: This methodology used difference reflectivity—$Z_{\mathrm{DP}} = 10\log_{10}(Z_H - Z_V)$, where Z_V is reflectivity from the vertical channel—to separate the liquid and ice contributions to Z_{H}. Then, reflectivity–mass relationships were used to estimate ice and liquid water mass separately for each grid point. It was difficult to quantify the error in these retrievals, but all the same lessons from the D_0 discussion would apply here as well. In addition, confidence intervals were computed similar to the D_0 methodology. Note that ice–liquid water mass retrievals necessarily only provided results for precipitation-sized particles, not cloud particles unobservable by the S-Pol.

Topographic data were obtained from a digital elevation model (DEM) that was matched to the radar grids, exactly as in Lang et al. (2007a) and Rowe et al. (2008). Terrain bands were broken down as follows: Gulf of California (over water; 12 726 grid points in the DEM), coastal plain (0–500 m MSL; 6713 grid points), 500–1500 m MSL (2934 grid points), and >1500 m MSL (4852 grid points). The land terrain bands roughly corresponded to the low, middle, and high elevation groups used for the NAME Event Rain Gauge Network (NERN)

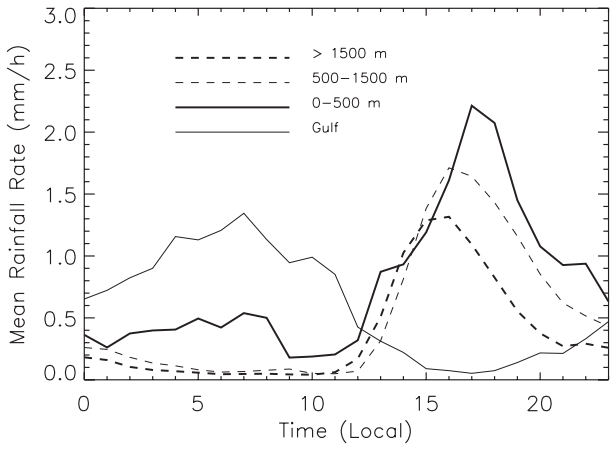

FIG. 2. Diurnal cycle of convective rainfall for S-Pol domain, broken down by terrain band.

data (Gochis et al. 2004). See Fig. 1 for the geographic distribution of these terrain bands.

Meteorological regimes (A, B, AB, and no regime) were defined exactly as in Lang et al. (2007a). Regime A consisted of enhanced rainfall over the Gulf and coastal plain, while regime B consisted of enhanced northward coast-parallel propagation of precipitation systems. These regimes typically overlapped, so their intersection, regime AB, was defined by Lang et al. (2007a) as well. ''No regime'' occurred when neither regime A nor regime B was active. Because of the common overlap between regimes A and B, there was little difference in results for regimes A, B, or AB versus no regime. Therefore, in this paper only results for regime AB (i.e., disturbed regime) versus no regime are presented. This is similar to how Lang et al. (2007a) presented their intraseasonal results.

3. Results

a. Results over the entire duration of the project

1) DIURNAL CYCLE OF CONVECTIVE RAINFALL

As a sanity check given the different radar and rain gauge datasets involved, the diurnal cycle of convective rainfall was calculated for each terrain band and compared to previous NAME rainfall studies (Fig. 2; Gochis et al. 2003, 2004, 2007; Lang et al. 2007a; Nesbitt et al. 2008; Rowe et al. 2008). The basic results seen in previous studies also were manifested in the S-Pol 3D dataset; that is, convective rainfall increased after noon local time in the highest terrain, and the rainfall maximum there led the maxima at lower elevations. However, there was a minor increase in coastal convective precipitation in the early afternoon, which was reflective of sea-breeze convection that typically occurred before the arrival of convection moving off the SMO. An early morning maximum in convective rainfall was observed over the Gulf, which also was associated with a relative maximum over the coastal plain around the same time.

While all of the above observations were consistent with the results of previous studies, one key difference in this study was that peak convective rain rates over the Gulf were relatively large. For instance, in Lang et al. (2007a) the maximum precipitation feature rainfall volume over the Gulf was significantly less than over the highest elevations of the SMO. A similar result in conditional-mean rainfall rate was seen in Rowe et al. (2008). Yet here, the maximum conditional-mean *convective* rainfall rate over the Gulf was essentially as intense as over the highest terrain.

This observation likely was due to a combination of two causes. One is that previous radar studies did not explicitly break down rainfall by convective and stratiform contributions. Thus, if light stratiform precipitation was relatively more common over the Gulf, then total rain rates would be depressed relative to convective rain rates. There is evidence that this was true, as Lang et al. (2007a) found that rainfall convective fraction during the Gulf rainfall peak (early morning) was less than the convective fraction during afternoon rainfall maxima in other terrain bands. A second cause is that Lang et al. (2007a) found early morning (i.e., Gulf) precipitation to be more common in the southern portion of the NAME 2D multiradar regional rainfall composites compared to the northern portion. Given that S-Pol observed the southern half of this domain, it is reasonable to conclude that S-Pol observed the majority of significant Gulf precipitation, and thus S-Pol-observed Gulf convective rainfall should be relatively more intense than Gulf rainfall included in a larger regional dataset.

2) DSD OBSERVATIONS

Because of the large number of samples provided by a 6-week project (hundreds of thousands), the 95% confidence intervals for mean D_0 retrievals typically were in the thousandths of a millimeter. Frequency distributions of near-surface D_0 reveal that the lowest frequency of large D_0 values (i.e., $D_0 > 2$ mm) occurred over the Gulf (Fig. 3). Meanwhile, over land, the frequency of large D_0 increased as elevation decreased. Mean D_0 over the Gulf was 1.32 mm, compared with 1.43 mm over the coastal plain, 1.36 mm in the 500–1500-m band, and 1.32 mm at >1500 m. Based on the 95% confidence intervals for the mean D_0 values, the small differences between the Gulf and the coastal plain—as well as between the highest terrain and the coastal plain—likely were significant.

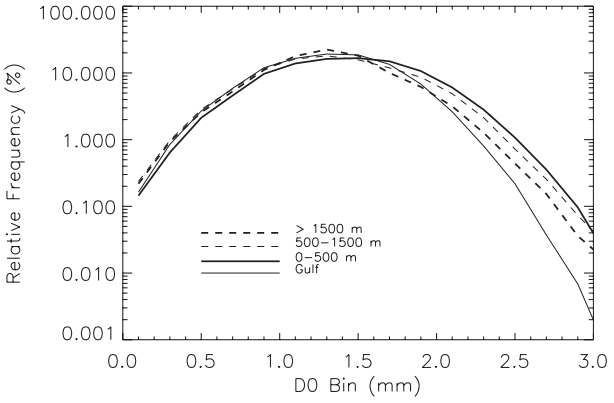

FIG. 3. Convective D_0 distributions by terrain band.

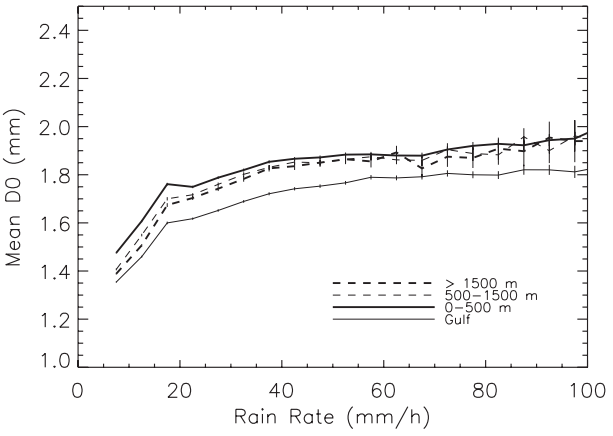

FIG. 4. Convective D_0 by rain rate vs terrain band. The 95% confidence intervals are indicated by vertical lines. Too few samples contained rates >100 mm h^{-1}, making confidence intervals too large for useful interpretation. Thus, these data are not shown.

These smaller D_0 values over the Gulf were, in general, consistently observed regardless of rainfall rate (Fig. 4). In other words, Gulf convection produced a given rainfall rate via a smaller D_0 compared to land convection, suggesting fundamental differences in DSDs between land and sea during NAME. At all terrain bands, the rate of increase of D_0 with rain rate slowed down considerably after 40 mm h^{-1}, suggesting that an equilibrium DSD (Hu and Srivastava 1995) was nearly achieved at these higher rain rates. This implied that, in intense rainfall, warm-rain precipitation processes were robustly developed and that collision, coalescence, and drop breakup were nearly balanced. The quasi-equilibrium D_0 values at higher rain rates were very similar among the land terrain bands (about 1.9 mm, versus ~1.8 mm over water).

3) ICE AND LIQUID WATER MASS

Conditional-mean vertical profiles of ice and liquid water mass demonstrated some key differences in convective structure as a function of terrain (Fig. 5). Throughout the vertical column, Gulf convection normally contained the least amount of ice mass, and ice mass in land convection typically increased as elevation decreased. Meanwhile, above 6 km MSL (about −5°C) Gulf convection contained the least amount of liquid water, but this quickly changed below the freezing-level altitude (about 5 km MSL during NAME), where closest to the surface it contained the most liquid water. Over land, coastal-plain convection contained the most liquid water regardless of altitude. However, in both coastal-plain and Gulf convection there were decreases in liquid water content near the surface.

There are a couple potential reasons for the near-surface decrease in liquid water over the coastal plain and Gulf. One is that the ice–liquid retrieval methodology was partially based on Z_H, and melting of large ice hydrometeors was commonly observed in intense NAME convection (Higgins et al. 2006). Thus, something akin to the "bright band" effect in stratiform precipitation (Austin and Bemis 1950), which increases Z_H in the melting zone relative to points below, likely existed in some NAME convection. As melting ice developed a liquid water coating, this may have positively biased the liquid water retrievals around 4 km MSL. S-Pol reflectivity profiles, which are currently being compared with satellite radar profiles, support this inference (Rutledge et al. 2009). However, note that no such signature occurred in the 500–1500-m MSL terrain band, despite it having the second-largest amount of ice mass aloft. Another potential explanation is subcloud evaporation. Based on their limited measurements, Nesbitt et al. (2008) suggested that subcloud evaporation should be most significant over the lowest terrain in this region, where the fall distance between cloud base and ground level is largest. In addition, a cross-coastal gradient in relative humidity at low levels also was shown by Johnson et al. (2010), especially in the afternoon and evening. However, as noted by Higgins and Gochis (2007), significant uncertainty exists regarding the structure of the humidity field in this region, making it difficult to accurately quantify the effect of subcloud evaporation.

The integrated ice and liquid water paths (IWP and LWP, respectively), based on the profiles in Fig. 5, are shown in Table 1. Clearly, the Gulf stood out from the land, with an IWP/LWP ratio of 0.40, compared to the land where it ranged from 0.56 to 0.60.

b. Intraseasonal results

1) DSD OBSERVATIONS

Overall, mean D_0 varied only 1–3 hundredths of a millimeter, regardless of terrain band, between regime

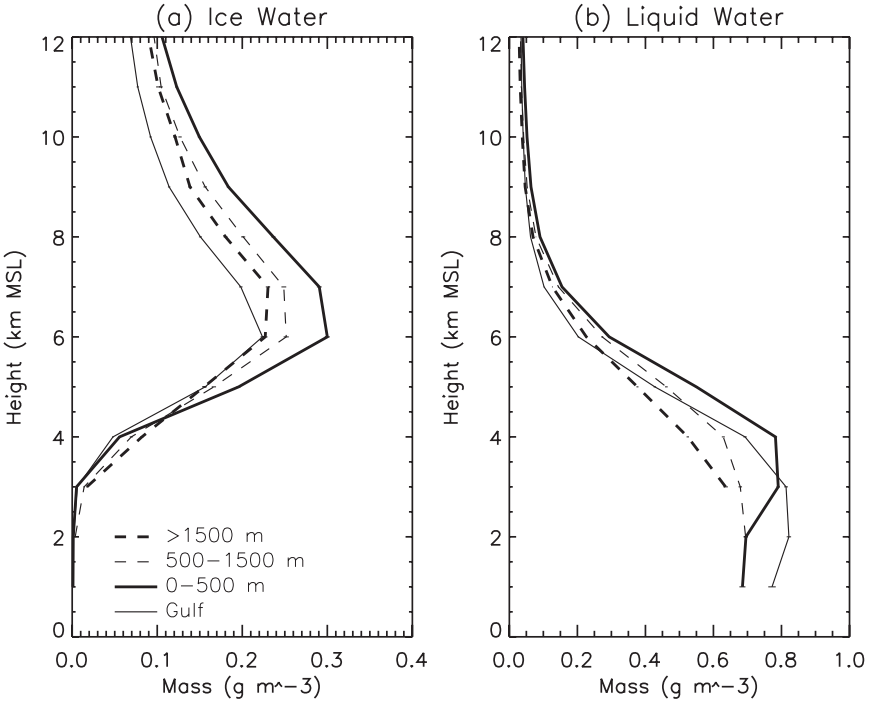

FIG. 5. (a) Vertical profiles of convective ice water mass by terrain band. The 95% confidence intervals are indicated by horizontal lines. (b) As in (a), but for convective liquid water mass.

AB and no regime. Therefore, no intraseasonal analog to Fig. 3 is shown, as these overall differences likely were not significant. However, there were interesting changes in D_0 as a function of rain rate for Gulf convection (Fig. 6). There was a general (and likely significant) tendency at many Gulf rain rates (<80 mm h^{-1}) for D_0 to be slightly smaller (by ~0.1 mm) during regime AB, compared to no regime. These differences were larger than any observed changes over land, as there were small decreases in D_0 at lighter rain rates (<50 mm h^{-1}) over the coastal plain and insignificant changes at higher elevations. The reduction in drop size is suggestive of increased maritime characteristics in convection over the Gulf (and possibly the coastal plain) during regime AB.

2) ICE AND LIQUID WATER MASS

At most terrain bands, and at most altitudes, convective ice water mass increased modestly during regime AB compared to no regime (Fig. 7). The largest percentage increase occurred over the Gulf, while the least change occurred in the >1500-m MSL terrain band. Over most terrain bands, the largest increases occurred in the heart of the mixed-phase region, around 6 km MSL. There was some evidence for decreases above 8–10 km MSL during regime AB, especially over the Gulf and the highest elevations. That is, whereas there may have been more precipitation-sized ice mass at lower altitudes over the Gulf during regime AB, there likely was less ice at higher altitudes.

Some of the most interesting differences between regime AB and no regime occurred in liquid water mass (Fig. 8). Over the Gulf, ice water mass increased at most by 25% depending on altitude (Fig. 7a), but liquid water mass near the surface nearly doubled during regime AB (Fig. 8a). In addition, during no regime there was a decrease in Gulf liquid water mass near the surface, but this signature was nearly eliminated during regime AB. This was consistent with either a reduction in subcloud evaporation or the elimination of a melting-ice signature in Z_H. However, the latter explanation would not be consistent with the observed increase in ice mass at lower altitudes over the Gulf (Fig. 7a). In addition, there is some evidence that relative humidity values were higher during regime AB compared to no regime, although this

TABLE 1. Mean convective ice water path (IWP), liquid water path (LWP), and their ratio for each terrain band, for the entire S-Pol deployment during NAME.

	IWP (kg m^{-2})	LWP (kg m^{-2})	IWP ÷ LWP
Gulf	1.62	4.10	0.40
0–500 m MSL	2.58	4.27	0.60
500–1500 m MSL	2.25	3.84	0.59
>1500 m MSL	2.17	3.85	0.56

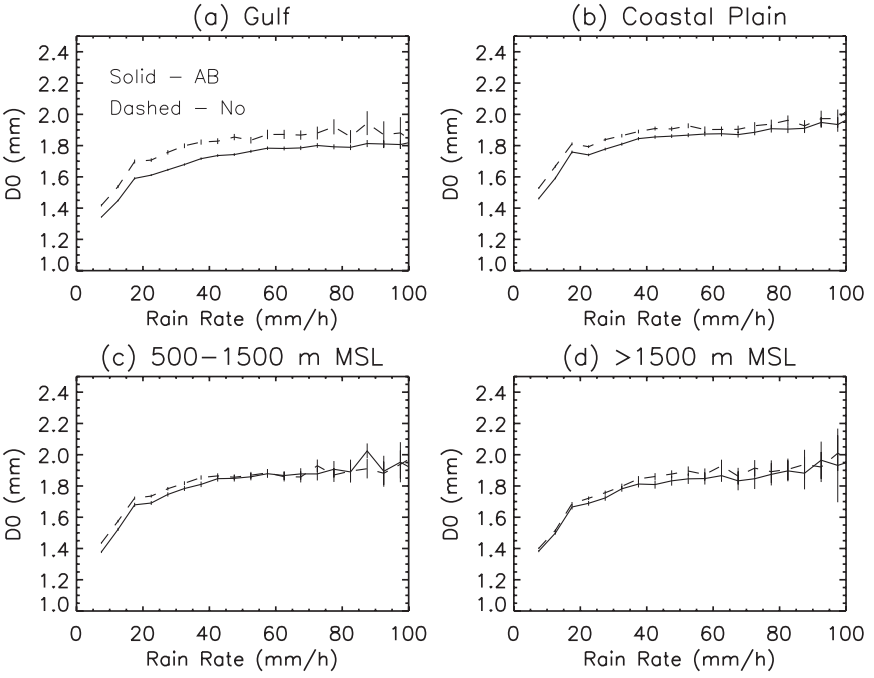

FIG. 6. Convective D_0 by rain rate vs regime AB and no regime. The 95% confidence intervals are indicated by vertical lines. (a) Gulf; (b) Coastal plain (0–500 m MSL); (c) 500–1500 m MSL; (d) >1500 m MSL.

signature was largest above 700 hPa (Lang et al. 2007a). Coastal-plain convection showed a similar increase in liquid water mass (especially near the surface) during regime AB, but not nearly as dramatically as Gulf convection. By contrast, very little change occurred in liquid water mass profiles at higher elevations, especially in the >1500-m terrain band.

Increases in liquid water mass in Gulf and coastal-plain convection were expected, given that regime AB was defined by increased rainfall over these regions. However, Figs. 7 and 8 point to significant microphysical changes in convection in these two regions during regime AB, especially compared to convection over the higher terrain (whose profiles barely changed). Over the Gulf, the massive increase in liquid mass—compared to the more modest increase in ice mass—suggested the amplified influence of warm-rain microphysical processes compared to ice-based ones, during disturbed meteorological regimes. The changes in coastal-plain convection also supported this same inference, though the change likely was not as dramatic. High-terrain convection, especially >1500 m MSL, was nearly unchanged regardless of meteorological regime.

4. Discussion and conclusions

This study reveals important spatial and temporal variability in the microphysical structure of convection during the NAME campaign. This documented variability has obvious implications for estimating rain rates, especially if these estimators are limited to traditional reflectivity–rainfall rate relationships. In the spatial sense, the primary mode of variability appeared to be between land and the Gulf of California, with secondary variability as a function of terrain height over land. On average, convection over the Gulf featured smaller D_0 values compared to convection over land, regardless of rain rate. This was coupled with reduced ice mass aloft relative to land convection. However, convection over the Gulf contained about as much rainfall as over the coastal plain, where the most intense convection resided. These results suggest that Gulf of California convection contained characteristics of maritime tropical convection—namely, increased importance of warm-rain collision and coalescence processes instead of ice-based precipitation processes, which typically results in smaller average drop sizes despite copious rainfall (Atlas and Ulbrich 2000, 2006; Bringi et al. 2003; Rosenfeld and Ulbrich 2003; Ulbrich and Atlas 2007; Bringi et al. 2009).

This result, which supports the thermodynamic analyses of Johnson et al. (2007, 2010), is remarkable given that the analysis domain for the S-Pol radar was narrow in the cross-coastal dimension (~320 km), with about half of that viewing the Gulf. Thus, these profound microphysical changes in convection occurred within a relatively narrow spatial range. Among other things, this has

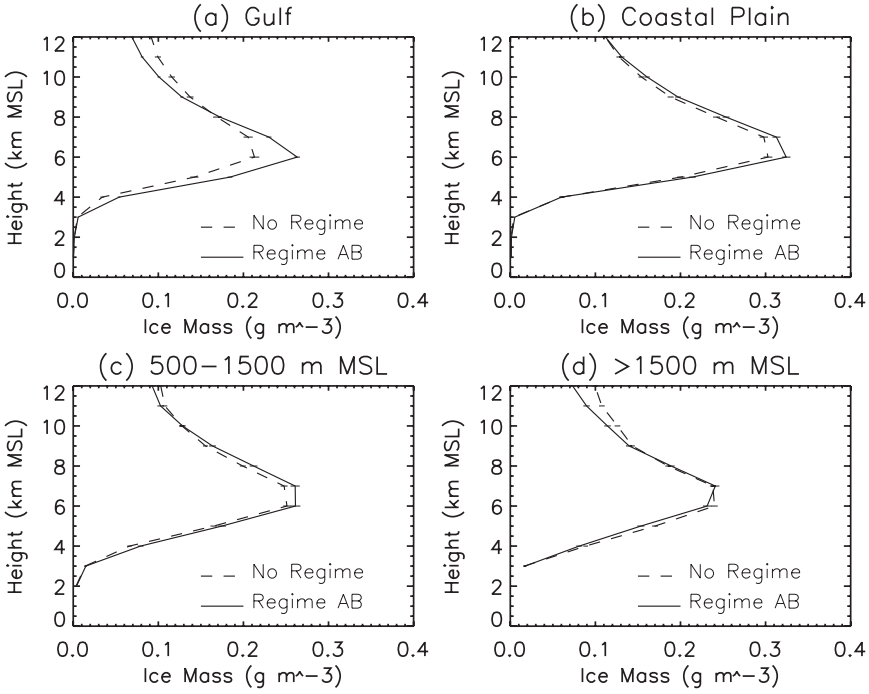

FIG. 7. As in Fig. 6, but for convective ice water mass profiles.

important implications for the accuracy of satellite precipitation retrievals in this region, as well as other locations that are subject to significant microphysical variability (Nesbitt et al. 2008).

Lang et al. (2007a) noted that precipitating systems over the Gulf generally had two different origins: 1) easterly propagating systems moving directly off the coast within the radar domain and 2) southerly propagating

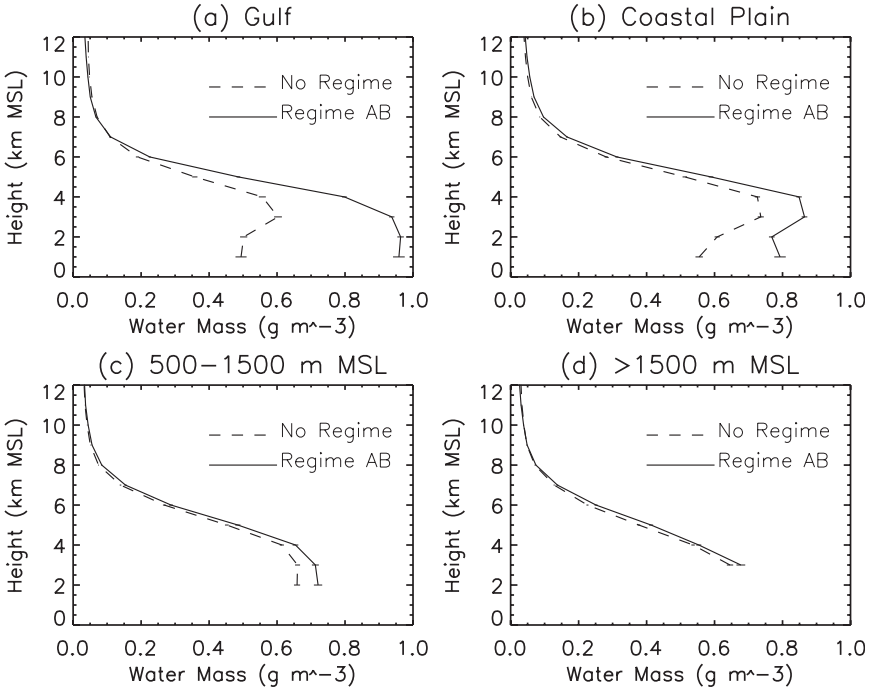

FIG. 8. As in Fig. 6, but for convective liquid water mass.

systems that moved parallel to the coast but that originated farther to the south, out of S-Pol radar range. The former systems typically occurred in the early evening, whereas the latter were common in the early morning hours. It is hypothesized that the latter systems, because of their longer residence times over open water (especially before moving into view of S-Pol) and thus longer exposure to maritime environmental conditions, were primarily responsible for the observed land–sea contrasts in this study. Testing this hypothesis is beyond the scope of this study, but it could be accomplished via individual case studies of NAME convective systems.

Over land, the polarimetric data suggested that convective intensity increased with decreasing elevation during NAME. This resulted in increased ice mass aloft, increased water mass and rainfall intensity near the surface, and often larger drop sizes over the coastal plain relative to the high terrain. This is completely consistent with the general interpretation of upscale development and organization of precipitating systems as they propagated from the high terrain toward the coast, during which one would expect average convective intensity and vertical development to increase (Johnson et al. 2007, 2010; Lang et al. 2007a; Nesbitt et al. 2008; Rowe et al. 2008). A potential explanation for this is that integrated buoyancy [i.e., convective available potential energy (CAPE)] increased with decreasing elevation, as a larger depth of unstable atmosphere was available to power convection.

Nesbitt et al. (2008) hypothesized that convection over the high terrain would have a shallower depth of cloud containing precipitation-sized ice compared to lower terrain. The results of this study confirm an overall reduced amount of precipitation-sized ice over the high terrain; however, this does not imply that warm-rain processes were dominant, as liquid water mass was similarly reduced and integrated IWP/LWP ratio was very similar to other land terrain bands. Rowe et al. (2008) suggested that increased warm-cloud depth over the coastal plain may have assisted in increasing rainfall intensity there, via additional cloud depth below the freezing level available for collision and coalescence. This interpretation is consistent with the present results; however, given the increased ice mass over the coastal plain it is likely that ice-based precipitation processes also played a role in enhancing rainfall intensity. Liquid-water profiles suggested that near-surface evaporation may have occurred over the Gulf and coastal plain, especially during undisturbed meteorological regimes, an observation supported by the limited humidity observations presented in Lang et al. (2007a), Nesbitt et al. (2008), and Johnson et al. (2010). However, in order to quantitatively evaluate this hypothesis, far better humidity measurements would be needed than were available during NAME (Higgins and Gochis 2007).

During disturbed meteorological regimes, the most pronounced convective differences occurred over the Gulf. While there was a modest increase in ice mass aloft, the liquid water mass nearly doubled near the surface. This was coupled with a slight reduction in average drop size and was suggestive of increased maritime characteristics within the Gulf convection during disturbed periods. This is unsurprising since these periods were in part defined by the existence of significant precipitating systems over the Gulf, many of which traveled over water from the south (Lang et al. 2007a). Similar but less dramatic changes occurred over the coastal plain.

Interestingly, during disturbed periods, the least-changed convection was over the highest terrain (especially >1500 m MSL). Whether in regime AB or no regime, DSDs along with ice and water mass remained nearly the same. This is consistent with the inference of Lang et al. (2007a) and Nesbitt et al. (2008) that high-terrain precipitating systems behaved similarly on a day-to-day basis during NAME. Convection typically formed in the early afternoon and propagated westward. The key change during disturbed periods was that these systems could survive past sunset, growing upscale into MCSs and other organized systems over the coastal plain and Gulf. Under this scenario, very little intraseasonal change would be expected in high-terrain convection, as observed in the present study.

While this study has shed some additional light on the microphysical structure of convection during NAME, it remains difficult to properly quantify the roles that ice-based microphysical growth, collision–coalescence, and evaporation play in producing observed rainfall rate distributions and DSDs in this region. Putting hard numbers with known uncertainties on these processes remains the next great step in this analysis, but one that is beyond the scope of this limited study. Perhaps some detailed case studies coupled with numerical modeling could play an important role in fleshing out these uncertainties.

As with most NAME-related studies, the present work would greatly benefit from having additional field seasons of S-Pol radar data to analyze, but unfortunately these data do not exist. Such data could quantify the representativeness of the 2004 monsoon while also opening additional avenues of analysis into interannual variability of convection in this region. The spatial and temporal resolution of the S-Pol dataset used in the present study was not ideal for examining the finescale structure and evolution of convection, particularly over the lifetime of individual cells. However, case studies of individual

convective elements during NAME using the higher-resolution ''storm evolution'' scan sets are ongoing and will be reported in future papers. Also underway are comparisons of the NAME field results with polarimetric radar data from other tropical regions—notably western Brazil, northern Australia, and western Africa—as well as the effects of observed microphysical variations on satellite precipitation retrieval algorithms.

Acknowledgments. This work greatly benefitted from contributions by Dave Ahijevych, Rit Carbone, Larry Carey, Dave Gochis, Paul Hein, Steve Nesbitt, Gustavo Pereira, Angela Rowe, and the NCAR S-Pol staff during NAME (led by Don Ferraro and Jon Lutz). This research was funded by the National Science Foundation via Grants ATM-0733396 and ATM-0340544.

REFERENCES

Adams, D. K., and A. C. Comrie, 1997: The North American monsoon. *Bull. Amer. Meteor. Soc.,* **78,** 2197–2213.

Atlas, D., and C. W. Ulbrich, 2000: An observationally based conceptual model of warm oceanic convective rain in the tropics. *J. Appl. Meteor.,* **39,** 2165–2181.

——, and C. R. Williams, 2003: The anatomy of a continental tropical convective storm. *J. Atmos. Sci.,* **60,** 3–15.

——, and C. W. Ulbrich, 2006: Drop size spectra and integral remote sensing parameters in the transition from convective to stratiform rain. *Geophys. Res. Lett.,* **33,** L16803, doi:10.1029/2006GL026824.

Austin, P. M., and A. C. Bemis, 1950: A quantitative study of the ''bright band'' in radar precipitation echoes. *J. Atmos. Sci.,* **7,** 145–151.

Boccippio, D. J., S. J. Goodman, and S. Heckman, 2000: Regional differences in tropical lightning distributions. *J. Appl. Meteor.,* **39,** 2231–2248.

——, W. A. Petersen, and D. J. Cecil, 2005: The tropical convective spectrum. Part I: Archetypal vertical structures. *J. Climate,* **18,** 2744–2769.

Bordoni, S., and B. Stevens, 2006: Principal component analysis of the summertime winds over the Gulf of California: A gulf surge index. *Mon. Wea. Rev.,* **134,** 3395–3414.

Bringi, V. N., and V. Chandrasekar, 2001: *Polarimetric Doppler Weather Radar: Principles and Applications*. Cambridge University Press, 636 pp.

——, ——, J. Hubbert, E. Gorgucci, W. L. Randeu, and M. Schoenhuber, 2003: Raindrop size distribution in different climatic regimes from disdrometer and dual-polarized radar analysis. *J. Atmos. Sci.,* **60,** 354–365.

——, C. R. Williams, M. Thurai, and P. T. May, 2009: Using dual-polarized radar and dual-frequency profiler for DSD characterization: A case study from Darwin, Australia. *J. Atmos. Oceanic Technol.,* **26,** 2107–2122.

Brito-Castillo, L., A. V. Douglas, A. Leyva-Contreras, and D. Lluch-Belda, 2003: The effect of large-scale circulation on precipitation and streamflow in the Gulf of California watershed. *Int. J. Climatol.,* **23,** 751–768.

Carey, L. D., and S. A. Rutledge, 2000: The relationship between precipitation and lightning in tropical island convection: A C-band polarimetric radar study. *Mon. Wea. Rev.,* **128,** 2687–2710.

Cetrone, J., and R. A. Houze, 2006: Characteristics of tropical convection over the ocean near Kwajalein. *Mon. Wea. Rev.,* **134,** 834–853.

Cifelli, R., W. A. Petersen, L. D. Carey, S. A. Rutledge, and M. A. F. da Silva Dias, 2002: Radar observations of kinematic, microphysical, and precipitation characteristics of two MCSs in TRMM LBA. *J. Geophys. Res.,* **107,** 8077, doi:10.1029/2000JD000264.

——, L. Carey, W. A. Petersen, and S. A. Rutledge, 2004: An ensemble study of wet season convection in southwest Amazonia: Kinematics and implications for diabatic heating. *J. Climate,* **17,** 4692–4707.

——, S. W. Nesbitt, S. A. Rutledge, W. A. Petersen, and S. Yuter, 2007: Radar characteristics of precipitation features in the EPIC and TEPPS regions of the east Pacific. *Mon. Wea. Rev.,* **135,** 1576–1595.

DeMott, C. A., and S. A. Rutledge, 1998: The vertical structure of TOGA COARE convection. Part I: Radar echo distributions. *J. Atmos. Sci.,* **55,** 2730–2747.

Douglas, M. W., R. A. Maddox, K. Howard, and S. Reyes, 1993: The Mexican monsoon. *J. Climate,* **6,** 1655–1677.

Fuller, R. D., and D. J. Stensrud, 2000: The relationship between tropical easterly waves and surges over the Gulf of California during the North American monsoon. *Mon. Wea. Rev.,* **128,** 2983–2989.

Gochis, D. J., J.-C. Leal, W. J. Shuttleworth, C. J. Watts, and J. Garatuza-Payan, 2003: Preliminary diagnostics from a new event-based precipitation monitoring system in support of the North American Monsoon Experiment. *J. Hydrometeor.,* **4,** 974–981.

——, A. Jimenez, C. J. Watts, J. Garatuza-Payan, and W. J. Shuttleworth, 2004: Analysis of 2002 and 2003 warm-season precipitation from the North American Monsoon Experiment Event Rain Gauge Network. *Mon. Wea. Rev.,* **132,** 2938–2953.

——, L. Brito-Castillo, and W. J. Shuttleworth, 2006: Hydroclimatology of the North American monsoon region in northwest Mexico. *J. Hydrol.,* **316,** 53–70.

——, C. J. Watts, J. Garatuza-Payan, and J. Cesar-Rodriguez, 2007: Spatial and temporal patterns of precipitation intensity as observed by the NAME Event Rain Gauge Network from 2002 to 2004. *J. Climate,* **20,** 1734–1750.

Hales, J. E., Jr., 1972: Surges of maritime tropical air northward over the Gulf of California. *Mon. Wea. Rev.,* **100,** 298–306.

Halverson, J. B., T. Rickenbach, B. Roy, H. Pierce, and E. Williams, 2002: Environmental characteristics of convective systems during TRMM-LBA. *Mon. Wea. Rev.,* **130,** 1493–1509.

Higgins, W., and D. Gochis, 2007: Synthesis of results from the North American Monsoon Experiment (NAME) Process Study. *J. Climate,* **20,** 1601–1607.

——, and Coauthors, 2006: The NAME 2004 field campaign and modeling strategy. *Bull. Amer. Meteor. Soc.,* **87,** 79–94.

Houze, R. A., and C. P. Cheng, 1977: Radar characteristics of tropical convection observed during GATE: Mean properties and trends over the summer season. *Mon. Wea. Rev.,* **105,** 964–980.

Hu, Z., and R. C. Srivastava, 1995: Evolution of raindrop size distribution by coalescence, breakup, and evaporation: Theory and observations. *J. Atmos. Sci.,* **52,** 1761–1783.

Johnson, R. H., T. M. Rickenbach, S. A. Rutledge, P. E. Ciesielski, and W. H. Schubert, 1999: Trimodal characteristics of tropical convection. *J. Climate,* **12,** 2397–2418.

——, P. E. Ciesielski, B. D. McNoldy, P. J. Rogers, and R. K. Taft, 2007: Multiscale variability of the flow during the North American Monsoon Experiment. *J. Climate,* **20,** 1628–1648.

——, ——, T. S. L'Ecuyer, and A. J. Newman, 2010: Diurnal cycle of convection during the 2004 North American Monsoon Experiment. *J. Climate,* **23,** 1060–1078.

Jorgensen, D. P., and M. A. LeMone, 1989: Vertically velocity characteristics of oceanic convection. *J. Atmos. Sci.,* **46,** 621–640.

Lang, T. J., R. Carbone, S. A. Rutledge, D. A. Ahijevych, and S. W. Nesbitt, 2006: NAME regional radar composites, version 2. Colorado State University Rep., 19 pp. [Available online at http://radarmet.atmos.colostate.edu/name/composites/readme_NAME_regional_radar_composites_v2.pdf.]

——, D. A. Ahijevych, S. W. Nesbitt, R. E. Carbone, S. A. Rutledge, and R. Cifelli, 2007a: Radar-observed characteristics of precipitating systems during NAME 2004. *J. Climate,* **20,** 1713–1733.

——, S. A. Rutledge, and R. Carbone, 2007b: NAME three-dimensional (3-D) low-resolution S-Pol radar grids, version 1. Colorado State University Rep., 12 pp. [Available online at http://radarmet.atmos.colostate.edu/name/pubs/readme_NAME_3D_SPol_grids_lowres_v1.pdf.]

——, S. W. Nesbitt, and L. D. Carey, 2009: On the correction of partial beam blockage in polarimetric radar data. *J. Atmos. Oceanic Technol.,* **26,** 943–957.

Lerach, D. G., S. A. Rutledge, C. R. Williams, and R. Cifelli, 2010: Vertical structure of convective systems in NAME 2004. *Mon. Wea. Rev.,* **138,** 1695–1714.

May, P. T., and A. Ballinger, 2007: The statistical characteristics of convective cells in a monsoon regime (Darwin, Northern Australia). *Mon. Wea. Rev.,* **135,** 82–92.

——, J. H. Mather, G. Vaughan, C. Jakob, G. M. McFarquhar, K. N. Bower, and G. G. Mace, 2008: The Tropical Warm Pool International Cloud Experiment. *Bull. Amer. Meteor. Soc.,* **89,** 629–645.

Miller, L. J., C. G. Mohr, and A. J. Weinheimer, 1986: The simple rectification to Cartesian space of folded radial velocities from Doppler radar sampling. *J. Atmos. Oceanic Technol.,* **3,** 162–174.

Mohr, C. G., and R. L. Vaughn, 1979: An economical approach for Cartesian interpolation and display of reflectivity factor data in three-dimensional space. *J. Appl. Meteor.,* **18,** 661–670.

Nesbitt, S. W., E. J. Zipser, and D. J. Cecil, 2000: A census of precipitation features in the tropics using TRMM: Radar, ice scattering, and lightning observations. *J. Climate,* **13,** 4087–4106.

——, R. Cifelli, and S. A. Rutledge, 2006: Storm morphology and rainfall characteristics of TRMM precipitation features. *Mon. Wea. Rev.,* **134,** 2702–2721.

——, D. J. Gochis, and T. J. Lang, 2008: The diurnal cycle of clouds and precipitation along the Sierra Madre Occidental observed during NAME-2004: Implications for warm season precipitation estimation in complex terrain. *J. Hydrometeor.,* **9,** 728–743.

Orville, R. E., and D. W. Spencer, 1979: Global lightning flash frequency. *Mon. Wea. Rev.,* **107,** 934–943.

Pereira, L. G., and S. A. Rutledge, 2006: Diurnal cycle of shallow and deep convection for a tropical land and an ocean environment and its relationship to synoptic wind regimes. *Mon. Wea. Rev.,* **134,** 2688–2701.

Petersen, W. A., and S. A. Rutledge, 2001: Regional variability in tropical convection: Observations from TRMM. *J. Climate,* **14,** 3566–3586.

——, S. W. Nesbitt, R. J. Blakeslee, R. Cifelli, P. Hein, and S. A. Rutledge, 2002: TRMM observations of intraseasonal variability in convective regimes over the Amazon. *J. Climate,* **15,** 1278–1294.

——, R. Cifelli, D. J. Boccippio, S. A. Rutledge, and C. Fairall, 2003: Convection and easterly wave structures observed in the eastern Pacific warm pool during EPIC-2001. *J. Atmos. Sci.,* **60,** 1754–1773.

Phillips, V. T. J., A. Pokrovsky, and A. Khain, 2007: The influence of time-dependent melting on the dynamics and precipitation production in maritime and continental storm clouds. *J. Atmos. Sci.,* **64,** 338–359.

Randell, S. C., S. A. Rutledge, R. D. Farley, and J. H. Helsdon Jr., 1994: A modeling study on the early electrical development of tropical convection: Continental and oceanic (monsoon) storms. *Mon. Wea. Rev.,* **122,** 1852–1877.

Rickenbach, T. M., R. N. Ferreira, J. B. Halverson, D. L. Herdies, and M. A. F. Silva Dias, 2002: Modulation of convection in the southwestern Amazon basin by extratropical stationary fronts. *J. Geophys. Res.,* **107,** 8040, doi:10.1029/2000JD000263.

Rosenfeld, D., and I. M. Lensky, 1998: Satellite-based insights into precipitation formation processes in continental and maritime convective clouds. *Bull. Amer. Meteor. Soc.,* **79,** 2457–2476.

——, and C. W. Ulbrich, 2003: Cloud microphysical properties, processes, and rainfall estimation opportunities. *Radar and Atmospheric Science: A Collection of Essays in Honor of David Atlas, Meteor. Monogr.,* No. 52, Amer. Meteor. Soc., 237–258.

Rowe, A. K., S. A. Rutledge, T. J. Lang, P. E. Ciesielski, and S. M. Saleeby, 2008: Elevation-dependent trends in precipitation observed during NAME. *Mon. Wea. Rev.,* **136,** 4962–4979.

Rutledge, S. A., E. R. Williams, and T. D. Keenan, 1992: The Down Upper Doppler and Electricity Experiment (DUNDEE): Overview and preliminary results. *Bull. Amer. Meteor. Soc.,* **73,** 3–16.

——, R. Cifelli, T. Lang, and S. W. Nesbitt, 2009: Contrasting tropical rainfall regimes using TRMM and ground-based polarimetric radar. *European Geosciences Union General Assembly 2009,* Vienna, Austria, EGU, AS1.3. [Available online at http://radarmet.atmos.colostate.edu/name/pubs/EGU_presentation_Rutledge.ppt.]

Silva Dias, M. A. F., and Coauthors, 2002: Cloud and rain processes in a biosphere–atmosphere interaction context in the Amazon Region. *J. Geophys. Res.,* **29,** 8072, doi:10.1029/2001JD000335.

Stith, J. L., J. E. Dye, A. Bansemer, A. J. Heymsfield, C. A. Grainger, W. A. Petersen, and R. Cifelli, 2002: Microphysical observations of tropical clouds. *J. Appl. Meteor.,* **41,** 97–117.

Takahashi, T., and K. Shimura, 2004: Tropical rain characteristics and microphysics in a three-dimensional cloud model. *J. Atmos. Sci.,* **61,** 2817–2845.

Tao, W.-K., and Coauthors, 2001: Retrieved vertical profiles of latent heat release using TRMM rainfall products for February 1998. *J. Appl. Meteor.,* **40,** 957–982.

——, and Coauthors, 2006: Retrieval of latent heating from TRMM measurements. *Bull. Amer. Meteor. Soc.,* **87,** 1555–1572.

——, S. Lang, X. Zeng, S. Shige, and Y. Takayabu, 2010: Relating convective and stratiform rain to latent heating. *J. Climate,* **23,** 1874–1893.

Toracinta, E. R., D. J. Cecil, E. J. Zipser, and S. W. Nesbitt, 2002: Radar, passive microwave, and lightning characteristics of precipitating systems in the tropics. *Mon. Wea. Rev.,* **130,** 802–824.

Ulbrich, C. W., and D. Atlas, 2007: Microphysics of raindrop size spectra: Tropical continental and maritime storms. *J. Appl. Meteor. Climatol.,* **46,** 1777–1791.

Wang, F. K., 2001: Confidence interval for the mean of non-normal data. *Qual. Reliab. Eng. Int.,* **17,** 257–267, doi:10.1002/qre.400.

Williams, C. R., and P. T. May, 2008: Uncertainties in profiler and polarimetric DSD estimates and their relation to rainfall uncertainties. *J. Atmos. Oceanic Technol.,* **25,** 1881–1887.

——, A. B. White, K. S. Gage, and F. M. Ralph, 2007: Vertical structure of precipitation and related microphysics observed by NOAA profilers and TRMM during NAME 2004. *J. Climate,* **20,** 1693–1712.

Williams, E. R., S. A. Rutledge, S. G. Geotis, N. Renno, E. Rasmussen, and T. Rickenbach, 1992: A radar and electrical study of tropical "hot towers." *J. Atmos. Sci.,* **49,** 1386–1395.

Xu, W., E. J. Zipser, and C. Liu, 2009: Rainfall characteristics and convective properties of mei-yu precipitation systems over South China, Taiwan and the South China Sea. Part I: TRMM observations. *Mon. Wea. Rev.,* **137,** 4261–4275.

Yuter, S. E., and R. A. Houze, 1998: The natural variability of precipitating clouds over the western Pacific warm pool. *Quart. J. Roy. Meteor. Soc.,* **124,** 53–99.

——, ——, E. A. Smith, T. T. Wilheit, and E. Zipser, 2005: Physical characterization of tropical oceanic convection observed in KWAJEX. *J. Appl. Meteor.,* **44,** 385–415.

Zipser, E. J., 1994: Deep cumulonimbus cloud systems in the tropics with and without lightning. *Mon. Wea. Rev.,* **122,** 1837–1851.

——, and K. R. Lutz, 1994: The vertical profile of radar reflectivity of convective cells: A strong indicator of storm intensity and lightning probability? *Mon. Wea. Rev.,* **122,** 1751–1759.